Impedance-Based Prediction of SSR-Generated Harmonics in Doubly-Fed Induction Generators

Preprint

Shahil Shah, Vahan Gevorgian, and Hanchao Liu

[1] *National Renewable Energy Laboratory*
[2] *GE Global Research Center*

Presented at the 2019 IEEE Power and Energy Society General Meeting (IEEE PES GM)
Atlanta, Georgia
August 4–8, 2019

NREL is a national laboratory of the U.S. Department of Energy
Office of Energy Efficiency & Renewable Energy
Operated by the Alliance for Sustainable Energy, LLC

This report is available at no cost from the National Renewable Energy Laboratory (NREL) at www.nrel.gov/publications.

Contract No. DE-AC36-08GO28308

Conference Paper
NREL/CP-5D00-72559
September 2019

Impedance-Based Prediction of SSR-Generated Harmonics in Doubly-Fed Induction Generators

Preprint

Shahil Shah,[1] Vahan Gevorgian,[1] and Hanchao Liu[2]

[1] *National Renewable Energy Laboratory*
[2] *GE Global Research Center*

Suggested Citation
Shah, Shahil, Vahan Gevorgian, and Hanchao Liu. 2019. *Impedance-Based Prediction of SSR-Generated Harmonics in Doubly-Fed Induction Generators: Preprint*. Golden, CO: National Renewable Energy Laboratory. NREL/CP-5D00-72559. https://www.nrel.gov/docs/fy19osti/72559.pdf.

NREL is a national laboratory of the U.S. Department of Energy
Office of Energy Efficiency & Renewable Energy
Operated by the Alliance for Sustainable Energy, LLC

This report is available at no cost from the National Renewable Energy Laboratory (NREL) at www.nrel.gov/publications.

Contract No. DE-AC36-08GO28308

Conference Paper
NREL/CP-5D00-72559
September 2019

National Renewable Energy Laboratory
15013 Denver West Parkway
Golden, CO 80401
303-275-3000 • www.nrel.gov

NOTICE

This work was authored in part by the National Renewable Energy Laboratory, operated by Alliance for Sustainable Energy, LLC, for the U.S. Department of Energy (DOE) under Contract No. DE-AC36-08GO28308. Funding provided by the U.S. Department of Energy Office of Energy Efficiency and Renewable Energy Water Power Technologies Office. The views expressed herein do not necessarily represent the views of the DOE or the U.S. Government. The U.S. Government retains and the publisher, by accepting the article for publication, acknowledges that the U.S. Government retains a nonexclusive, paid-up, irrevocable, worldwide license to publish or reproduce the published form of this work, or allow others to do so, for U.S. Government purposes.

Cover Photos by Dennis Schroeder: (clockwise, left to right) NREL 51934, NREL 45897, NREL 42160, NREL 45891, NREL 48097, NREL 46526.

Impedance-Based Prediction of SSR-Generated Harmonics in Doubly-Fed Induction Generators

Shahil Shah[1], Vahan Gevorgian[1], and Hanchao Liu[2]

[1]National Renewable Energy Laboratory (NREL)
Golden, CO 80401, USA
Email: Shahil.Shah@nrel.gov, Vahan.Gevorgian@nrel.gov

[2]GE Global Research Center
Niskayuna, NY 12309, USA
Email: Hanchao.Liu@ge.com

***Abstract*–Doubly-fed induction generators (DFIGs) are prone to subsynchronous resonance (SSR) with series-compensated transmission lines and experiencing SSR-generated harmonics of wide-ranging magnitudes. This paper presents a large-signal impedance-based approach for the prediction of the magnitude of SSR-generated harmonics in DFIGs. Note that the large-signal impedance of a network shows variation in its impedance response with the magnitude of perturbation at its terminals. It is discovered in this paper that the impedance of a series-compensated transmission line starts changing with the magnitude of SSR because of the metal-oxide varistor-based protection of series capacitors in the line. The changing line impedance halts the growth of the SSR beyond a certain point, where the DFIG forms a limit-cycle mode and emits harmonics at the SSR frequency. The discovered role of the protection of series capacitors in SSR not only enables the prediction of SSR-generated harmonics but also can be used for the timely detection of an SSR event to avoid system disruption and sudden loss of bulk generation. The large-signal impedance-based prediction of SSR-generated harmonics in DFIG-based wind and hydro generators is demonstrated using numerical simulations of a 2.5-MVA, 690-V DFIG supplying to a series-compensated transmission line.**

Index Terms–**DFIG, hydro generators, wind turbines, series-compensated transmission lines, SSR, MOV, impedance analysis.**

I. Introduction

Doubly fed-induction generators (DFIGs) with back-to-back voltage source converters (VSCs) is an attractive topology for applications demanding variable-speed operation of generators [1]. DFIGs are widely used in wind turbines, and they are being increasingly considered for small hydro generators. One major concern with the grid integration of DFIGs is that they are prone to severe subsynchronous resonance (SSR) problems when they supply directly to a series-compensated transmission line [2]–[4]. The impedance-based analysis is proven effective at explaining the underlying mechanism of the SSR of DFIGs [5], [6]. It is shown that the inductive behavior of a DFIG in the subsynchronous frequency range caused by the machine inductance interacts with the capacitive impedance of the series-compensated line. The damping of the resulting SSR mode is typically low and sometimes becomes negative because of the so-called induction generator effect and the active controls of the rotor-side converter (RSC) and grid-side converter (GSC) [6]. Small-signal impedance-based modeling and analysis also supports the development of damping methods for resonance problems [7]; however, it cannot predict the magnitude of resonance-generated harmonics. SSR-generated harmonics in DFIGs have resulted in disruption in many power systems around the world: a) the magnitude of SSR-generated voltage harmonics reached as high as 2 p.u. in Texas, United States in 2009 [2]; and b) tens of SSR events were observed more recently in the Hebei Province of China, which hosts almost 3.5 GW of wind power, more than 80% of which comes from DFIG turbines [4]. The magnitudes of SSR-generated harmonics are found to vary sporadically depending on the number of wind turbines in operation and wind speed. It is important to be able to predict the magnitude of these SSR-generated harmonics and understand the factors governing them for the protection design of DFIGs and timely detection of SSR; timely detection and fast corrective action is one of the most efficient approaches for avoiding disruptions caused by SSR [8].

This paper presents an impedance-based approach for the prediction of the magnitude of SSR-generated harmonics in a DFIG supplying to a series-compensated transmission line. The paper applies recently developed large-signal impedance theory for the prediction of resonance-generated harmonics [9]. It is shown that the impedance of the line starts changing with the SSR magnitude because of the activation of the surge protection of series capacitors using metal-oxide varistors (MOV) [10]; this halts the growth of SSR beyond a certain point, where the DFIG enters into a limit-cycle mode with sustained harmonics at the SSR frequency. The role of the MOV in the SSR of DFIGs discovered in this paper not only helps predict the magnitude and frequency of SSR-generated harmonics but also can be used for the timely detection of an SSR event by monitoring the voltage across MOVs across the series capacitors of the compensated line.

II. Small-Signal Impedance Analysis of SSR in DFIGs

Fig. 1 shows circuit diagram and control implementation of a 2.5-MVA, 0.69-kV DFIG used in this paper to demonstrate the prediction of the SSR magnitude. The current references for the dq current control of the RSC are regulated by outer active power/speed and reactive power control loops. Because the bandwidths of these outer-loop controls are limited to a few hertz, they do not affect the DFIG dynamics in the subsynchronous frequency range

This work was authored by Alliance for Sustainable Energy, LLC, the manager and operator of the National Renewable Energy Laboratory for the U.S. Department of Energy (DOE) under Contract No. DE-AC36-08GO28308. Funding provided by U.S. Department of Energy Office of Energy Efficiency and Renewable Energy Water Power Technologies Office. The views expressed in the article do not necessarily represent the views of the DOE or the U.S. Government. The U.S. Government retains and the publisher, by accepting the article for publication, acknowledges that the U.S. Government retains a nonexclusive, paid-up, irrevocable, worldwide license to publish or reproduce the published form of this work, or allow others to do so, for U.S. Government purposes.

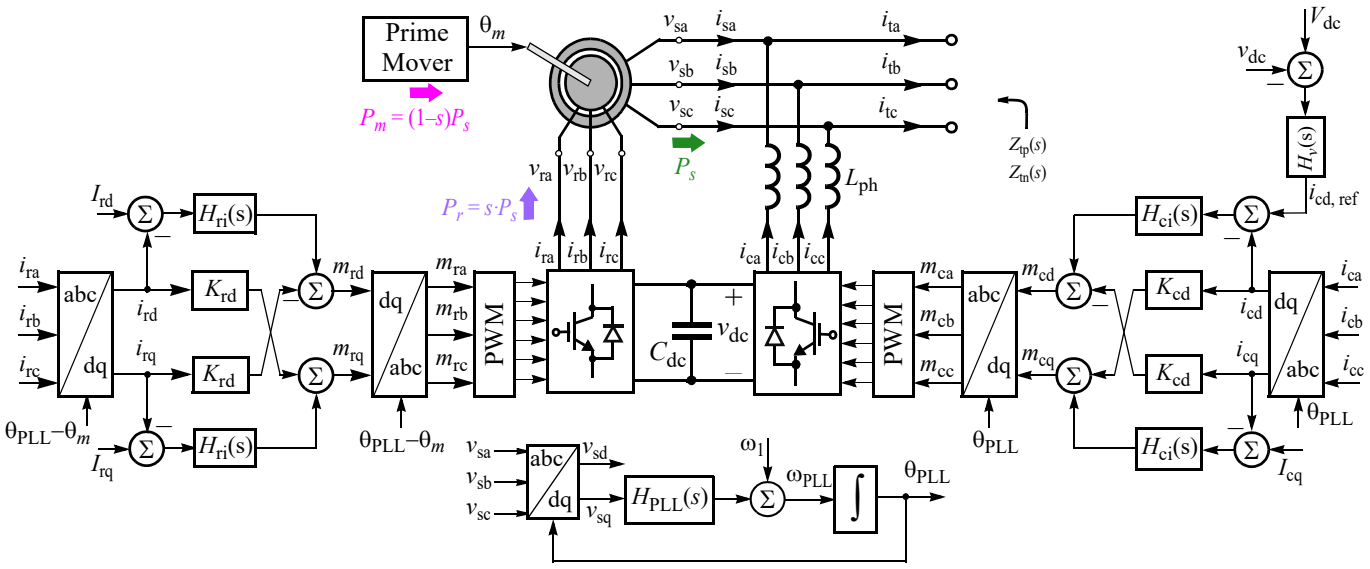

Fig. 1. Circuit and control diagram of a doubly-fed induction generator (DFIG).

TABLE I PARAMETERS AND OPERATION CONDITION OF A DFIG FOR PSCAD SIMULATIONS

Parameter	Value	Parameter	Value
Rated Power, S	2.5 MVA	Rated Voltage, V	690 V
Rated Frequency, f_1	60 Hz	DC Voltage, V_{dc}	2000 V
Stator to Rotor Turns Ratio, N_s/N_r	0.37912	PCC Voltage (peak), V_1	690 sqrt(2/3)
Stator Resistance, R_s	0.0054 p.u.	Rotor Resistance, R_r	0.00607 p.u.
Stator Leakage Inductance, L_{ls}	0.102 p.u.	Rotor Leakage Inductance, L_{lr}	0.110 p.u.
Magnetizing Inductance, L_m	4.362 p.u.	GSC Reactor Inductance, L_{ph}	0.2 p.u.
PWM Gain, k_m	0.5	DC-Bus Capacitance, C_{dc}	20 mF
RSC Current Controller, $H_{ri}(s)$	$(0.455+50.51/s)\cdot 10^{-3}$	RSC Decoupling gain, K_{rd}	$92.6\text{x}10^{-6}$
GSC Current Controller, $H_{gi}(s)$	$(0.27+338.4/\text{i})\cdot 10^{-3}$	RSC Decoupling gain, K_{gd}	$113.1\text{x}10^{-6}$
Rotor Speed, ω_m	1.33 p.u.	Rotor Speed (Electrical), f_m	80 Hz
PLL Compensator, $H_{PLL}(s)$	$0.236+44.59/s$	DC-Bus Controller, $H_v(s)$	$-(4.205+528.53/s)$
RSC O/P Current, $I_{rd}+j\cdot I_{rq}$	$1148-j\cdot 257$	GSC O/P Current, $I_{cd}+j\cdot I_{cq}$	$977-j\cdot 0$

and they are ignored in this paper. Hence, the current references, I_{rd} and I_{rq}, to the RSC are kept constant, and the prime mover is represented by an ideal speed source. The GSC regulates the dc-bus voltage, v_{dc}, by regulating the d-axis component, i_{cd}, of its output currents, $i_{c,abc}$. The q-axis component, i_{cq}, of $i_{c,abc}$ is regulated to control the reactive power output from the GSC. Table I shows DFIG parameters and operation condition used for the PSCAD simulations and analysis presented in this paper.

A. Sequence Impedance Modeling of a DFIG

Impedance modeling of VSCs, including cross-coupling between the positive and negative sequence impedances, and between the ac- and dc-side networks, is presented in [11]. The only challenge in the impedance modeling of a DFIG is evaluating how the RSC impedance is mapped to the stator side through the induction machine [6]. The mapping of the stator-side perturbations to the rotor side and vice versa involves frequency-dependent scaling factors as well as a shift in their frequencies. An added complexity is that the scaling factor and frequency shift are different for the positive and negative sequence perturbations. These mappings are represented in Fig. 2 using an equivalent circuit of the induction machine. Factors $\sigma_p(s)$ and $\sigma_n(s)$ in Fig. 2 are frequency-dependent gains given by:

$$\sigma_p(s) = \frac{s - j\omega_m}{s} \text{ and } \sigma_n(s) = \frac{s + j\omega_m}{s} \quad (1)$$

As in [6], the dc-bus voltage control dynamics and the coupling between the positive and negative sequence impedances are ignored because they affect the accuracy of the developed models only at frequencies closer to the fundamental frequency [11]. With these approximations, the positive-sequence impedance of the DFIG, $Z_{tp}(s)$, can be obtained as the parallel combination of the positive-sequence

$$Z_{\text{sp}}(s) \equiv -\frac{V_{\text{sp}}(s)}{I_{\text{sp}}(s)} = \frac{R_s + \dfrac{R_r'}{\sigma_p(s)} + s(L_{\text{ls}} + L_{\text{lr}}') + k_m V_{\text{dc}} \left(\dfrac{N_s}{N_r}\right)^2 \left[\dfrac{H_{\text{ri}}(s - j\omega_1) - jK_{\text{rd}}}{\sigma_p(s)}\right]}{1 - \dfrac{T_{\text{PLL}}(s - j\omega_1)}{2} \dfrac{k_m V_{\text{dc}}}{\sigma_p(s)} \dfrac{N_s}{N_r} \left\{ \dfrac{\mathbf{M}_{\text{rl}}}{V_1} + [H_{\text{ri}}(s - j\omega_1) - jK_{\text{rd}}] \dfrac{\mathbf{I}_{\text{rl}}}{V_1} \right\}}$$

$$Z_{\text{cp}}(s) \equiv -\frac{V_{\text{sp}}(s)}{I_{\text{cp}}(s)} = \frac{sL_{\text{ph}} + k_m V_{\text{dc}} [H_{\text{ci}}(s - j\omega_1) - jK_{\text{cd}}]}{1 - \dfrac{T_{\text{PLL}}(s - j\omega_1)}{2} \left[1 + \dfrac{\mathbf{I}_{\text{cl}}}{V_1} k_m V_{\text{dc}} H_{\text{ci}}(s - j\omega_1)\right]} \tag{3}$$

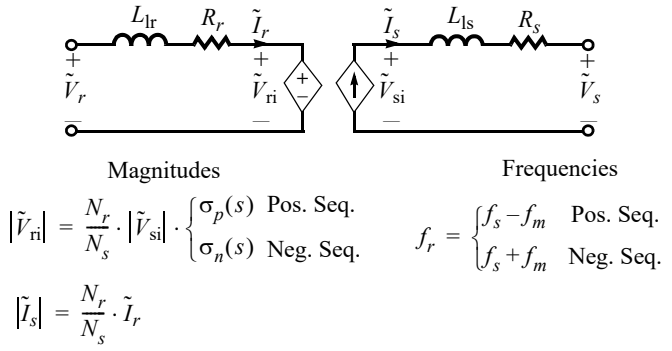

Fig. 2. Equivalent circuit of induction machine showing mapping of positive and negative sequence perturbation components between stator and rotor.

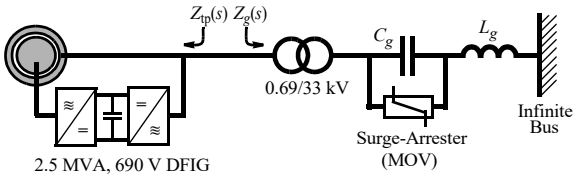

Fig. 3. 2.5-MVA DFIG supplying to a series-compensated transmission line.

impedances of the induction machine including the RSC dynamics, $Z_{\text{sp}}(s)$, and the GSC, $Z_{\text{cp}}(s)$:

$$Z_{\text{tp}}(s) = \frac{Z_{\text{sp}}(s) \cdot Z_{\text{cp}}(s)}{Z_{\text{sp}}(s) + Z_{\text{cp}}(s)} \tag{2}$$

Using the equivalent circuit in Fig. 2 and the harmonic linearization method, $Z_{\text{sp}}(s)$ and $Z_{\text{gp}}(s)$ are obtained as shown in (3), where $T_{\text{PLL}}(s) = [V_1 \cdot H_{\text{PLL}}(s)/s] \cdot [1 + V_1 \cdot H_{\text{PLL}}(s)/s]^{-1}$ is the closed-loop gain of the PLL, and $\mathbf{M}_{\text{rl}}$, $\mathbf{I}_{\text{rl}}$, and $\mathbf{I}_{\text{cl}}$ are respectively the steady-state values of $m_{r,\text{abc}}$, $i_{r,\text{abc}}$, and $i_{c,\text{abc}}$ in the phasor form, for instance $\mathbf{M}_{\text{rl}} = M_{\text{rd}} + jM_{\text{rq}}$.

B. SSR with Series-Compensated Transmission Line

Fig. 3 shows the DFIG supplying to a series-compensated transmission line. The short-circuit ratio (SCR) of the uncompensated line is 4 for the base of 50 MVA, 33 kV. Series capacitors provide 50% compensation and increase the SCR to 8. Note that the small-signal grid impedance seen by the DFIG is given by:

$$Z_g(s) = (0.69/33)^2 \cdot [sL_g + 1/(sC_g)] \tag{4}$$

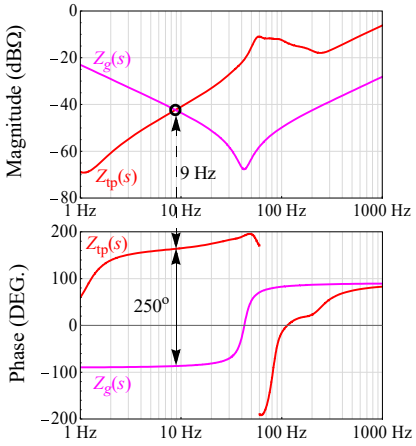

Fig. 4. Small-signal impedance-based stability analysis of the 2.5-MVA DFIG supplying to a series-compensated transmission line.

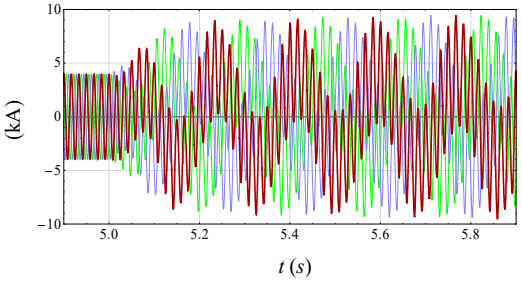

Fig. 5. DFIG output currents during subsynchronous resonance.

Fig. 4 compares the small-signal impedance responses of the DFIG and grid obtained using (2)–(4). It predicts an unstable SSR at 9 Hz with the phase margin of –70° (=180°–250°). As shown in Fig. 5, dynamic simulations indeed confirm SSR after the series capacitors are inserted at 5 s; however, based on the frequency spectrum of the DFIG output currents shown in Fig. 6, the frequency of the SSR-generated harmonics is 5.5 Hz instead of 9 Hz predicted by the small-signal impedance analysis in Fig. 4. Additionally, the small-signal impedance analysis cannot predict the magnitude of the SSR-generated harmonics, which is 3.85 kA based on the spectrum shown in Fig. 6. Note that the SSR-generated harmonics are of almost the same magnitude as the rated current output at the fundamental frequency before the insertion of the series capacitors. In addition to almost 1 p.u. of SSR-generated harmonics at 5.5 Hz, Fig. 6 shows a small component at 114.5 Hz, which is because of the cross-coupling

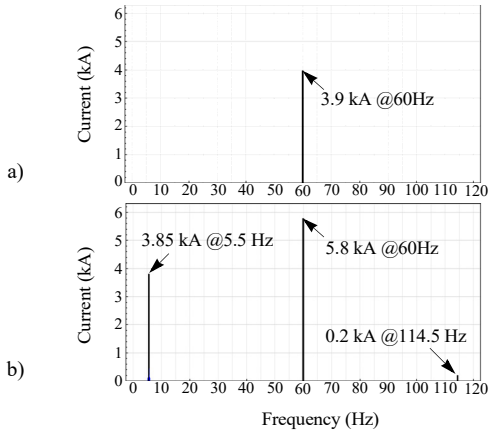

Fig. 6. Frequency components in the DFIG output currents before and after the insertion of series capacitors for 50% compensation. a) before the insertion of capacitors, b) after the insertion of capacitors.

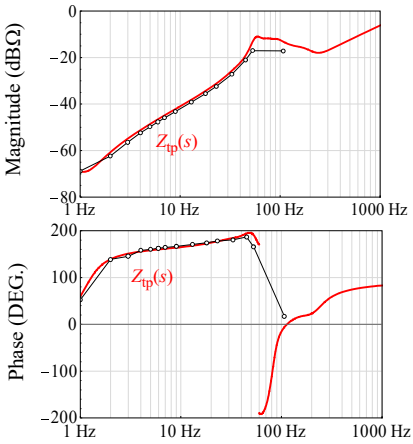

Fig. 7. Large-signal impedance response of the DFIG. Solid lines: small-signal impedance model prediction, dots: measured impedance response using point-by-point simulations for the injection of 100% current perturbation.

between the positive and negative sequence dynamics [11]. Fig. 6 also shows that during SSR, the fundamental component of the DFIG output currents has substantially increased to 5.8 kA from the pre-SSR value of 3.9 kA.

III. Large-Signal Impedance-Based Prediction of the Magnitude of SSR-Generated Harmonics

Based on the large-signal impedance theory [9], the magnitude of the SSR-generated harmonics can be determined by comparing the large-signal impedance response of the DFIG and the grid. Note that the large-signal impedance of any network represents its impedance responses for different magnitudes of the perturbation at its terminals. The impedance of the DFIG in Fig. 1 is measured for different values of the injected current perturbation magnitudes using numerical simulations. As shown in Fig. 7, the DFIG impedance in the subsynchronous frequency range does not change from the small-signal impedance response even when the injected current perturbation magnitude is increased as high as 1 p.u. Hence, based on the large-signal impedance theory [9], the growth of the SSR is not arrested by a change in the DFIG

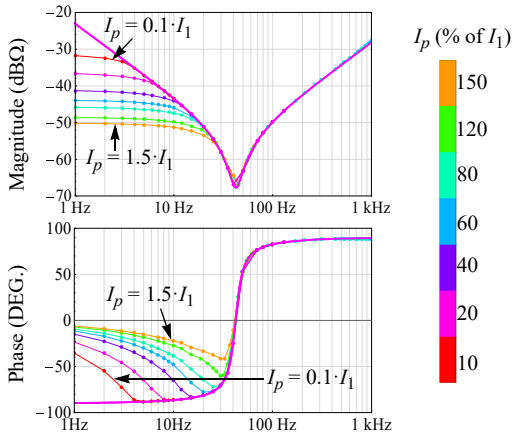

Fig. 8. Large-signal impedance of grid. Pink solid lines: small-signal impedance response, lines with dots: point-by-point simulations for different levels of the injected current perturbation, I_p.

impedance with the resonance magnitude. In other words, an unstable SSR will continue to grow indefinitely, until it triggers some protection, unless the growth of SSR is arrested by a change in the grid impedance with the SSR magnitude. This is precisely what is discovered in this paper: the grid impedance starts changing with the SSR magnitude and locks the growth of SSR at a certain point. The insensitivity of the DFIG impedance to the injected perturbation magnitude emphasizes the linearity of the DFIG dynamics. This is because the dynamics of the induction machine dominates the DFIG impedance, which are substantially "more" linear than the dynamics of the power converters [12].

The large-signal impedance of the grid is measured using simulations by injecting current perturbations of different magnitudes. The injected positive-sequence current perturbations are superimposed on the fundamental current output from the DFIG. The measured grid impedance responses for different current perturbations magnitudes, I_p, are shown in Fig. 8. The change in the grid impedance with the perturbation magnitude, I_p, is explained in the following.

The MOV-based surge protection across the series capacitors, as shown in Fig. 3, protects the series capacitors from overvoltages. MOV is essentially a nonlinear resistor whose resistance reduces rapidly to a low value if the voltage across it starts increasing beyond a threshold level. Hence, whenever the voltage across a series capacitor increases beyond the threshold level because of the injected current perturbation, the MOV across it gets activated and partially bypasses the series-capacitor. Note that the perturbation current causes a higher voltage drop across series capacitors at low frequencies because of the higher impedance of the capacitors. This is why the grid impedance becomes more and more resistive in the subsynchronous frequency range, as shown in Fig. 8, as the injected current perturbation magnitude, I_p, is increased. The MOV does not react to high-frequency perturbations because the impedance of the series capacitors is much lower and most of the voltage drop appears across grid inductance, L_g.

Fig. 9 compares the large-signal impedance response of the grid with the DFIG impedance. Once the SSR starts growing at 9 Hz because of the negative phase margin of –70°, the grid

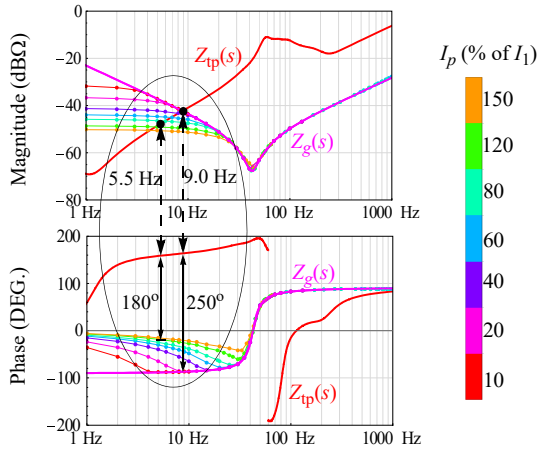

Fig. 9. Large-signal impedance-based prediction of the magnitude and frequency of SSR-generated harmonics. Analysis predicts SSR-generated harmonics at 5.5 Hz with the current magnitude of around 100% (1.0 p.u.).

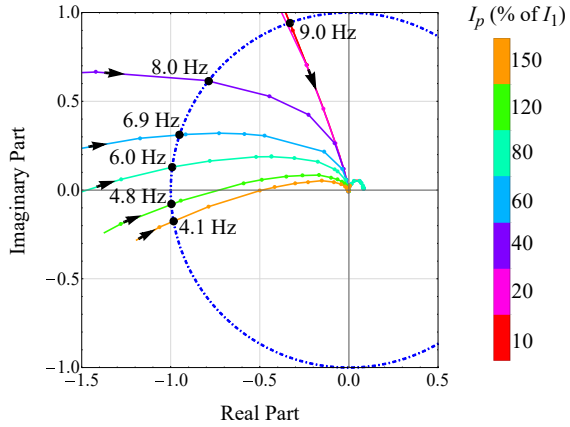

Fig. 10. Nyquist plot of $Z_g(s)/Z_{tp}(s)$ for different magnitudes of current perturbations (oscillations) at the interface of the DFIG and grid.

impedance starts changing. Because of the change in both the magnitude and phase responses of the grid impedance with the SSR magnitude, the impedance interaction frequency starts reducing and the phase margin starts increasing. Once the phase margin increases to zero – that is the phase difference between the grid impedance and the DFIG impedance at the interaction frequency becomes 180° – the resonance stops growing. Essentially, at this point, the DFIG enters a stable limit cycle and emits sustained SSR-generated harmonics. Based on the large-signal impedance analysis shown in Fig. 9, the DIFG will experience SSR-generated harmonics of around 100% magnitude (i.e., 1 p.u.) in its output currents at 5.5 Hz. The SSR-generated harmonics in the voltages at the DFIG terminals can be readily obtained by multiplying the current harmonics with the grid impedance at the resonance frequency. The prediction of the SSR-generated harmonics using the large-signal impedance analysis shown in Fig. 9 matches those observed in simulations; the frequency spectrum of the DFIG output currents during SSR in Fig. 6 also shows SSR-generated harmonics of around 1 p.u. at 5.5 Hz.

Fig. 10 shows large-signal impedance analysis using nyquist plots of the impedance ratio $Z_g(s)/Z_{tp}(s)$ for different magnitudes of current perturbation, I_p. It is evident that the nyquist plot starts changing with the resonance magnitude; it stops encircling the critical point –1+j0 once the resonance in the DFIG currents reached approximately 100%. Also, note the change in the frequency at which the nyquist plot enters the unit circle for different magnitudes of current perturbation.

IV. Conclusions

This paper applied large-signal impedance-based theory for the prediction of the magnitude and frequency of SSR-generated harmonics in DFIGs supplying to a series-compensated transmission line. It is discovered that the MOV-based surge protection of series capacitors in the compensated line changes the grid impedance with the SSR magnitude. This halts the growth of SSR beyond a certain point, which decides the magnitude and frequency of the SSR-generated harmonics a DFIG will experience. Future work will use the proposed approach to optimize the DFIG control system and protection to reduce the magnitude of SSR-generated harmonics under conditions where SSR cannot be completed eliminated. Future work will also develop a fast detection method of SSR events using voltage measurements across the MOV protection of series capacitors.

References

[1] G. Abad, J. Lopez, M. A. Rodriguez, L. Marroyo, and G. Iwanski, *Doubly-Fed Induction Machine – Modeling and Control for Wind Energy Generation*. Piscataway, NJ: IEEE Press/John WILEY and Sons, 2011.

[2] L. C. Gross, "Subsynchronous grid conditions: new event, new problem, and new solutions," in *Proc. Western Protective Relay Conf.*, Spokane, WA, 2010, pp. 1-19.

[3] K. Narendra, D. Fedirchuk, R. Midence, N. Zhang, A. Mulawarman, P. Mysore, and V. Sood, "New microprocessor based relay to monitor and protect power systems against sub-harmonics," in *Proc. 2011 IEEE Elect. Power and Energy Conf.*, pp. 438-443, 2011.

[4] X. Xie, X. Zhang, H. Liu, H. Liu, Y. Li, and C. Zhang, "Characteristic analysis of subsynchronous resonance in practical wind farms connected to series-compensated transmissions," *IEEE Trans. Energy Conv.*, vol. 32, no. 3, pp. 1117-1126, Sep. 2017.

[5] Z. Miao, "Impedance-model-based SSR analysis for type 3 wind generator and series-compensated network," *IEEE Trans. Energy Conv.*, vol. 27, no. 4, pp. 984-991, Dec. 2012.

[6] I. Vieto and J. Sun, "Sequence impedance modeling and analysis of type-III wind turbines," *IEEE Trans. Energy Conv.*, vol. 33, no. 2, pp. 537-545, June 2018.

[7] H. Liu and J. Sun, "Voltage stability and control of offshore wind farms with ac collection and HVDC transmission," *IEEE J. Emerg. Sel. Topics Power Electron.*, vol. 2, no. 4, pp. 1181-1189, Dec. 2014.

[8] "Lesson Learned – Sub-synchronous interaction between series-compensated transmission lines and generation," NERC, Atlanta, GA, USA, July 2011.

[9] S. Shah and L. Parsa, "Large-signal impedance for the analysis of sustained resonance in grid-connected converters," in *Proc. 2017 IEEE 18th Workshop on Control and Modeling for Power Electron. (COMPEL)*, Stanford, CA.

[10] Medium-Voltage Surge Arresters — Product Guide," Siemens AG, Erlangen, Germany, Catalogue HG 31.1, 2017.

[11] S. Shah and L. Parsa, "Impedance modeling of three-phase voltage source converters in DQ, sequence, and phasor domains," *IEEE Trans. Energy Conv.*, vol. 32, no. 3, pp. 1139-1150, April 2017.

[12] S. Shah, P. Koralewicz, V. Gevorgian, and R. Wallen, "Large-signal impedance modeling of three-phase voltage source converters," in *Proc. 44the Annual Conf. IEEE Ind. Electron. Soc. (IECON)*, Washington, DC, Oct. 2018.